Charge-carrier photogeneration in single-component organic carbazole-based semiconductors via low excitation power triplet-triplet annihilation

Andrei Stankevych, Rishabh Saxena, Jeannine Grüne, Sebastian Lulei, Andreas Sperlich, Stavros Athanasopoulos, Alexander Vakhnin, Prakhar Sahay, Wolfgang Brütting, Vladimir Dyakonov, Heinz Bässler, Anna Köhler, Andrey Kadashchuk

Angaben zur Veröffentlichung / Publication details:

Stankevych, Andrei, Rishabh Saxena, Jeannine Grüne, Sebastian Lulei, Andreas Sperlich, Stavros Athanasopoulos, Alexander Vakhnin, et al. 2023. "Charge-carrier photogeneration in single-component organic carbazole-based semiconductors via low excitation power triplet-triplet annihilation." *Physical Review Applied* 20 (6): 064029. https://doi.org/10.1103/physrevapplied.20.064029.

Editors' Suggestion

Charge-carrier photogeneration in single-component organic carbazole-based semiconductors via low excitation power triplet-triplet annihilation

Andrei Stankevych,[1,2,‡] Rishabh Saxena,[1,‡] Jeannine Grüne,[3,4] Sebastian Lulei,[3] Andreas Sperlich,[3] Stavros Athanasopoulos,[5] Alexander Vakhnin,[2] Prakhar Sahay,[6] Wolfgang Brütting,[6] Vladimir Dyakonov,[3] Heinz Bässler,[7] Anna Köhler,[1,7] and Andrey Kadashchuk[1,2,*,†]

[1] *Soft Matter Optoelectronics and Bavarian Polymer Institute (BPS), University of Bayreuth, Universitätsstr. 30, 95448 Bayreuth, Germany*

[2] *Institute of Physics, National Academy of Sciences of Ukraine, Prospect Nauky 46, 03028 Kyiv, Ukraine*

[3] *Experimental Physics VI and Würzburg-Dresden Cluster of Excellence ct.qmat, Julius-Maximilians-Universität Würzburg, 97074 Würzburg, Germany*

[4] *Cavendish Laboratory, University of Cambridge, JJ Thomson Avenue, Cambridge CB3 0HE, UK*

[5] *Departamento de Física, Universidad Carlos III de Madrid, Avenida Universidad 30, Leganés, 28911 Madrid, Spain*

[6] *Institute of Physics, University of Augsburg, Universitätsstr. 1, 86159 Augsburg, Germany*

[7] *Bayreuth Institute of Macromolecular Research (BIMF), University of Bayreuth, Universitätsstr. 30, 95448 Bayreuth, Germany*

(Received 11 September 2023; revised 6 November 2023; accepted 16 November 2023; published 15 December 2023)

It is generally believed that intrinsic charge generation via an autoionization mechanism in pristine single-component organic semiconductors is impossible upon photoexcitation within the lowest excited singlet state due to the large exciton binding energy. However, we present measurements of thermally stimulated luminescence, light-induced ESR, and photocurrent in the carbazole-based molecule 3′,5-di(9*H*-carbazol-9-yl)-[1,1′-biphenyl]-3-carbonitrile (mCBP-CN) films, revealing that charge-carrier pairs are efficiently produced upon excitation near their absorption edges. The photocurrent measurements show a superlinear dependence on the cw-photoexcitation intensity even at very low excitation power (below 1 mW/cm^2), suggesting a bimolecular nature of the charge photogeneration process. The photocurrent measured over a broad temperature range of 5–300 K exhibits a prominent maximum at moderately low temperature around 170 K and rolls off significantly at higher temperatures. This correlates remarkably with the maximum of delayed fluorescence induced by bimolecular triplet-triplet annihilation (TTA), i.e., triplet fusion, in this material. This behavior implies that the photocurrent is governed mainly by the TTA-induced production of geminate pairs and only a little by their subsequent dissociation. Moreover, we find that the field-assisted dissociation probability of photogenerated charge pairs becomes almost temperature-independent at temperatures below 100 K. This can be quantitatively described using a charge dissociation model accounting for the energy disorder and the distribution of geminate-pair radii. The key conclusion of this study is that triplet fusion can promote the energy up-conversion (to 5.42 eV), thereby enabling the autoionization of a high-energy neutral excited state. This serves as the predominant mechanism of intrinsic photogeneration in this single-component heavy-atom-free system. We attribute the effect to efficient intersystem crossing in mCBP-CN, a high triplet energy level (2.71 eV), and very long-lived triplet excitations. A broader implication of this finding is that the so far neglected mechanism of TTA-facilitated charge-carrier generation might be relevant for organic long-persistent luminescence materials, and even for organic photovoltaics and potentially for photocatalytic water splitting processes.

DOI: 10.1103/PhysRevApplied.20.064029

I. INTRODUCTION

Triplet-triplet annihilation (TTA) is a common bimolecular process that can occur in any organic solids where the high density of spin-triplet excitons and their ability to diffuse facilitate a non-negligible encounter probability during their (long) lifetime. Efficient photon energy up-conversion (UC) enabled by TTA under low excitation intensities is a well-established phenomenon for organic *two-component systems* employing heavy metal organic complexes as triplet sensitizers [1–5]. This implies the population of a singlet excited state via fusion of

*Corresponding author. kadash@iop.kiev.ua
†andriy.kadashchuk@uni-bayreuth.de
‡Authors contributed equally to this work

two lower-energy triplet excitons sensitized by embedded triplet "sensitizers" in a fluorescent "emitter" host material. Because these triplet sensitizers exhibit a high triplet population at room temperature, the TTA-UC in such composite films can occur at continuous-wave (cw)-excitation intensities as low as around 1 mW/cm^2 of noncoherent light. Therefore, such bimolecular energy UC is of interest for various photonic applications [6–8]. It is particularly interesting for organic solar cells, since it potentially enhances the efficiency of photovoltaic devices. The efficiency increase occurs, for example, by utilizing near-infrared photons beyond the band gap of solar cells via their UC to visible light [9] or by limiting triplet-related nonradiative losses [10,11]. The TTA-UC process is also viewed as an alternative or complementary mechanism to thermally activated delayed fluorescence and phosphorescence emitter strategies of utilizing the nonemissive triplets in organic light-emitting diode (OLED) devices [12–14], which may also solve the problem of the "efficiency roll-off" associated with these devices. Moreover, considering the easily tunable excitation and/or emission wavelength and low power excitation, the TTA-UC organic systems can be especially promising for photocatalytic water splitting to produce hydrogen [15], as they could be combined with a variety of photocatalysts that are only photoactive under ultraviolet light or in the short-wavelength region of visible light. In this study, we highlight another intriguing application of TTA as a major mechanism of intrinsic photocurrent (PC) generation in a *single-component*, heavy-atom-free annihilator medium, showing self-TTA. This mechanism has just recently been suggested for the single-component metal-organic complex of platinum(II) octaethylporphyrin (PtOEP) containing a heavy atom [16].

It is generally established that thermally stimulated luminescence (TSL) [17] and light-induced electron spin resonance (LESR) techniques [18,19] are valuable tools for probing trapped charge carriers in organic semiconductors. Of particular relevance is that both are electrode-free techniques that allow the separation of interface or contact effects from intrinsic bulk effects and do not require good charge transport in the material. Moreover, these techniques can be applied at very low temperature, enabling the characterization of even very shallow charge trapping. A lesser-known aspect of their use is that the action spectra of TSL and LESR signals could also provide essential information regarding charge-carrier photogeneration mechanisms in these materials [20,21]. Indeed, the LESR action spectra measured in films of the conjugated polymers of cyano-substituted poly(*p*-phenylene vinylene) (CN-PPV) and poly(2-methoxy,5-(2′-(ethyl-hexyloxy)-*p*-phenylene vinylene) (MEH-PPV) have demonstrated a clear threshold behavior at energies significantly exceeding the energy of the lowest singlet exciton (S_1) transition, which was found to match well with the PC action spectra reported for PPV derivatives [22]. The latter was attributed to intrinsic bulk charge-carrier photogeneration and the observed energy offset relative to the absorption spectra can provide an estimate for the exciton binding energy.

Similar behavior has been observed for the action spectra of TSL measured for various PPV derivatives [20,23]; namely, the TSL signal drastically increased with increasing excitation photon energy well above the $S_0 \rightarrow S_1$ absorption edge of these polymers. Thus, since TSL in organic semiconductors is believed to arise from the recombination of long-range geminate charge-carrier pairs [17,24,25], the TSL action spectra can be used to assess the carrier photogeneration efficiency in response to excitation photon energy. It is important to note that TSL probes geminate pairs generated predominantly through intrinsic photogeneration. This is because (i) TSL excludes electrode-sensitized charge photogeneration, in contrast to the thermally stimulated current technique [26], and (ii) any geminate pairs generated extrinsically via exciton dissociation at incidental (most likely acceptor-like) impurities, such as oxygen, are expected to recombine nonradiatively at impurity moieties that serve as recombination centers and thus make no contribution to the TSL signal. Despite this, some organic semiconductors, such as ladder-type methyl-substituted poly(phenylene), poly(*N*-vinyl carbazole), and different polyfluorene derivatives, show a surprisingly strong TSL under excitation at the optical absorption edge, with no appreciable dependence of TSL intensity on excitation photon energy above the optical gap [17,24]. This phenomenon has so far remained unresolved.

The present study was motivated by an intriguing recent observation of strong TSL signals under excitation *at the optical absorption edge* in pristine amorphous films of a large set of small-molecule carbazole-based OLED host materials [25,27], implying efficient carrier photoproduction within the lowest excited singlet state in *single-component* materials. This work focuses on 3′,5-di(9*H*-carbazol-9-yl)-[1,1′-biphenyl]-3-carbonitrile (mCBP-CN), a common wide-band-gap host material for blue emitters in OLEDs owing to its high triplet level, which was chosen here as an exemplary material exhibiting a significant phosphorescence emission at low temperatures. For comparison purposes, we also measured the TSL action spectra in a regioregular poly-3-hexylthiophene (rr-P3HT), chosen as a *representative counterexample*, i.e., a well-known nonphosphorescent material [28]. We found that the TSL of rr-P3HT behaves fundamentally differently, featuring a significant energy offset (0.6–0.7 eV) of the onset of its TSL action spectrum with respect to the absorption edge.

To clarify the mechanism of charge photogeneration in neat mCBP-CN films, we undertake a comprehensive study employing a range of techniques, including PL spectroscopy, LESR, PL-detected magnetic resonance (PLDMR), and PC measurements. We demonstrate that a large population of triplet excitons and concomitant

efficient TTA-UC occurring even at very low cw-excitation intensities lead to the autoionization of a high-energy neutral excited state. This is the dominant mechanism of geminate-pair generation in this material. In contrast, there is no noticeable population of triplets in rr-P3HT films owing to its very low intersystem crossing (ISC) rate upon excitation within the S_1 excited state. Accordingly, this results in negligible intrinsic charge generation. Hence, charge generation in mCBP-CN films is a bimolecular process, as evidenced by the observed supralinear dependence of the PC upon excitation intensity. Its efficiency exhibits the temperature dependence characteristic of the TTA process, namely peaking at moderately low temperatures and drastically decreasing when approaching room temperature because of progressively enhanced monomolecular triplet quenching by impurities. Concomitantly, the PC is observed only at low temperatures, and exhibits a prominent maximum at 170 K. This maximum is found to be mainly determined by the TTA-induced geminate-pair generation process. In contrast, the temperature dependence of the dissociation probability for the TTA-induced geminate pair is found to play a secondary role. In fact, we find that the field-assisted dissociation probability is surprisingly almost temperature independent at low temperatures $T \leq 100$ K, which can be well described within a charge dissociation model by accounting for the presence of energy disorder and longer-distance geminate pairs.

II. EXPERIMENT

A. Materials

mCBP-CN [see Fig. 1(a)] was purchased from Lumtec Corp. and used as received. For spectroscopy measurements, thin films of the mCBP-CN are spin-coated from 20-mg/ml chloroform solutions onto cleaned fused quartz substrates (1000 rpm, 30 s) that typically result in 50-nm-thick layers. Subsequently, the deposited films are dried in an oven at 40 °C for 10 min and then under vacuum for 2 h to remove residual solvent. For photocurrent measurements, mCBP-CN films are vacuum evaporated with a typical thickness of 150 nm. Photodiode devices with evaporated mCBP-CN active layers have a conventional configuration of glass/ITO(90 nm)/poly (3,4-ethylenedioxythiophene):poly(styrenesulfonic acid) (PEDOT:PSS)(25 nm)/mCBP-CN(150 nm)/LiF(0.5 nm)/ Al(100 nm).

B. Optical spectroscopy measurements

Steady-state absorption and PL spectra are measured using a double-beam Shimadzu 2450 UV-VIS spectrophotometer and a Jasco FP-8600 spectrofluorometer equipped with a Xe arc lamp (150 W) as an excitation light source. The spectrofluorometer also allows PL measurements in phosphorescence mode, for which the excitation light is chopped, the detector unit is opened at a delay of 50 ms after excitation, and the signal is acquired for 100 ms. For the 77 K measurements, the sample is immersed in liquid nitrogen. Photoluminescence quantum yield (PLQY) is measured using an integrating sphere coupled to the spectrofluorometer.

Time-resolved PL measurements are made using a setup consisting of a spectrograph coupled to a gated intensified charge-coupled device (ICCD) camera (Andor iStar 334) for acquiring emission spectra with distinct delay and integration time, where samples are excited with a frequency-tripled Nd:YAG laser (Innolas SpitLight 600) with a wavelength of 355 nm (3.5 eV). All experiments are performed with the sample in a temperature-controlled continuous flow helium cryostat (Oxford Instruments OptistatCF).

C. Photocurrent measurements

Stationary PC measurements are conducted in the same temperature-controlled helium cryostat, using excitation from a 1200-W Xe arc lamp coupled to a double-grating monochromator for wavelength selection. The temperature

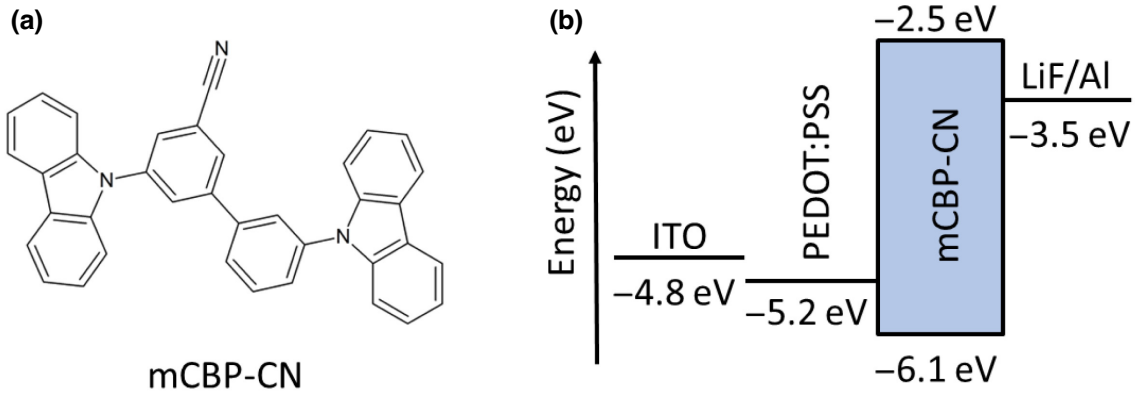

FIG. 1 (a) Molecular structure of mCBP-CN, (b) schematic energy levels diagram of investigated mCBP-CN single-layer photodiode.

dependence of the PC is measured at a weak cw-excitation power (0.54 mW/cm^2) at 355 nm. To measure the excitation intensity dependence of the PC, we employ an appropriate set of neutral density filters. PC action spectra are measured at a reverse bias of −7 V and using a lock-in technique for signal detection. To ensure that the PC has stabilized and is representative, we wait for 15 s after each monochromator advance and take several averages. The PC action spectrum is then corrected to account for the effective absorption spectrum of the mCBP-CN layer embedded in the device [Fig. 1(b)]. We calculate the effective absorption spectrum by using a transfer matrix approach implemented by Burkhard *et al.* [29]. The real and imaginary part of the refractive index, n and k, were measured for mCBP-CN by Naqvi *et al*. [30] using Sentec SE 850 Spectroscopic Ellipsometry along with SPECTRARAY software for the fitting. For other layer materials, we use the values provided in Ref. [29].

D. Thermally stimulated luminescence measurements

TSL is the phenomenon of light emission arising after the removal of excitation (UV light, in our case) under conditions of increasing temperature. Generally, in the TSL method, the trapping states are first populated by the photogeneration of charge carriers, usually at low temperatures. After terminating the excitation, the trapped charge carriers can be released by heating the sample and the luminescence due to charge recombination is recorded as a function of temperature. TSL measurements are carried out using a homebuilt system over a temperature range from 5 to 300 K using an optical temperature-regulating helium cryostat (see Ref. [27] for more details). More specifically, after cooling to 5 K, the samples are photoexcited, usually for 30 s, with a high-pressure 500-W mercury lamp with an appropriate set of glass optical filters for light selection, or with a UV LED emitting at 274 nm. After that, the samples are kept in the dark at a constant temperature (5 K) during a certain dwell time (typically 15 min) before the TSL heating run begins to allow the long isothermal afterglow (arising due to isothermal recombination of short-range geminate pairs) to decay to a negligible value. Then TSL measurements are started upon heating the sample from 5 to 300 K with a linear heating ramp (at constant heating rate, $\beta = 0.15$ K/s). TSL emission is detected with a cooled photomultiplier tube operated in photon-counting mode, attached to the cryostat window. We also measure the TSL action spectra; namely, the dependence of the integrated TSL intensity, i.e., the area under the TSL glow curve, upon the photon energy of excitation ($E_{h\upsilon}$). Since the TSL intensity may nonlinearly depend on the intensity of the incident light, the photon flux from different emissive lines of the mercury lamp used for TSL excitation is balanced by an appropriate attenuation of the stronger lines. Finally, the spectral range of the TSL emission is roughly estimated using a set of glass cutoff filters, as demonstrated in Ref. [31].

E. Light-induced ESR and PL-detected magnetic resonance

PLDMR and LESR experiments are carried out with a modified X-band spectrometer (Bruker E300) equipped with a continuous-flow helium cryostat (Oxford ESR 900) and a microwave cavity (Bruker ER4104OR, approximately 9.43 GHz) with optical access. Optical excitation is performed with either a 305-nm or 365-nm UV LED through the aperture in the cavity. Generally, PLDMR probes the microwave-induced PL changes at the resonance magnetic field for triplets or charges. For PLDMR, PL is detected with a silicon photodiode (Hamamatsu S2281), using a 355-nm or 409-nm long-pass filter to suppress the excitation light. The PL signal is amplified by a current and/or voltage amplifier (Femto DHPCA-100) and recorded by a lock-in amplifier (Ametek SR 7230), referenced by on-off-modulating the microwaves with a modulation frequency of 517 Hz. The microwaves are generated with a microwave signal generator (Anritsu MG3694C), amplified to 3 W (Microsemi), and guided into the cavity. For LESR spectra and transients, a microwave bridge (Bruker ER 047 MRP) provides microwave power up to 200 mW. An arbitrary waveform generator (Keithley 3390) provides 100-kHz sinusoidal field modulation superimposed onto the main magnetic field, referencing the lock-in amplifier. For transient LESR, the lock-in time constant is set to 100 ms to not influence the detected signal decay times. For LESR studies, a small amount of the mCBP-CN solution is poured into an ESR tube and vacuum dried, leaving a film of mCBP-CN on the tube wall. For PLDMR samples, the same spin-coated films used for optical spectroscopy are used by inserting them into ESR tubes. All ESR tubes are finally sealed under a helium atmosphere.

III. RESULTS

A. Spectroscopic and photocurrent measurements

A basic spectroscopical characterization of mCBP-CN films is shown in Fig. 2. For comparison, Fig. 2 also presents measurements for P3HT, which is chosen as a representative counterexample, i.e., a well-known nonphosphorescent material [28]. The steady-state PL emission spectrum of a mCBP-CN film is depicted by the blue solid curve in Fig. 2(a) and reveals both fluorescence and phosphorescence components clearly seen under cw-excitation at 77 K. The fluorescent component is characterized by a relatively broad structureless band peaking at 405 nm, which is a consequence of the charge transfer (CT)-character of the lowest singlet state of mCBP-CN due to presence of an acceptor

CN group. The latter also results in a slightly lower energy of the singlet state in this material, whose 0–0 transition is very close to the onset of emission at $S_1 = 3.30$ eV, as compared to mCBP films ($S_1 = 3.47$ eV) [33] devoid of such a CN group. The phosphorescence component dominates the delayed emission [blue dashed curve in Fig. 2(a)] measured using the same excitation light. In contrast to the fluorescence, the phosphorescence features a well-resolved vibronic structure of the $T_1 \rightarrow S_0$ emission spectrum with the 0–0 vibrational transition at $T_1 = 2.71$ eV, similar to that observed in mCBP films. As has been demonstrated before [33], such phosphorescence has been attributed to triplet excitation localized on the central biphenyl core in meta-linked carbazole-biphenyl materials, rather than on the carbazole moiety of such molecules, which has also been supported by quantum chemical calculations [34]. It is noteworthy that the phosphorescence of mCBP-CN films is readily visible even in steady-state PL spectra at 77 K; it appears as additional narrower peaks in the range $\lambda > 450$ nm superimposed on the broad fluorescence band [blue solid curve in Fig. 2(a)], implying a quite efficient ISC process in this material. Using the PLQY value of 11% (at 293 K) we measure in the mCBP-CN films, the ISC rate is estimated as $k_{ISC} = 1.8 \times 10^8$ s^{-1}, which is higher than the radiative rate of singlet excitations, $k_r^S = 2.1 \times 10^7$ s^{-1}, in this material. The delayed emission also reveals a delayed fluorescence (DF) component identical to the prompt fluorescence with a maximum at 405 nm [Fig. 2(a) dashed blue curve], which originates from the TTA process, as will be shown in the following.

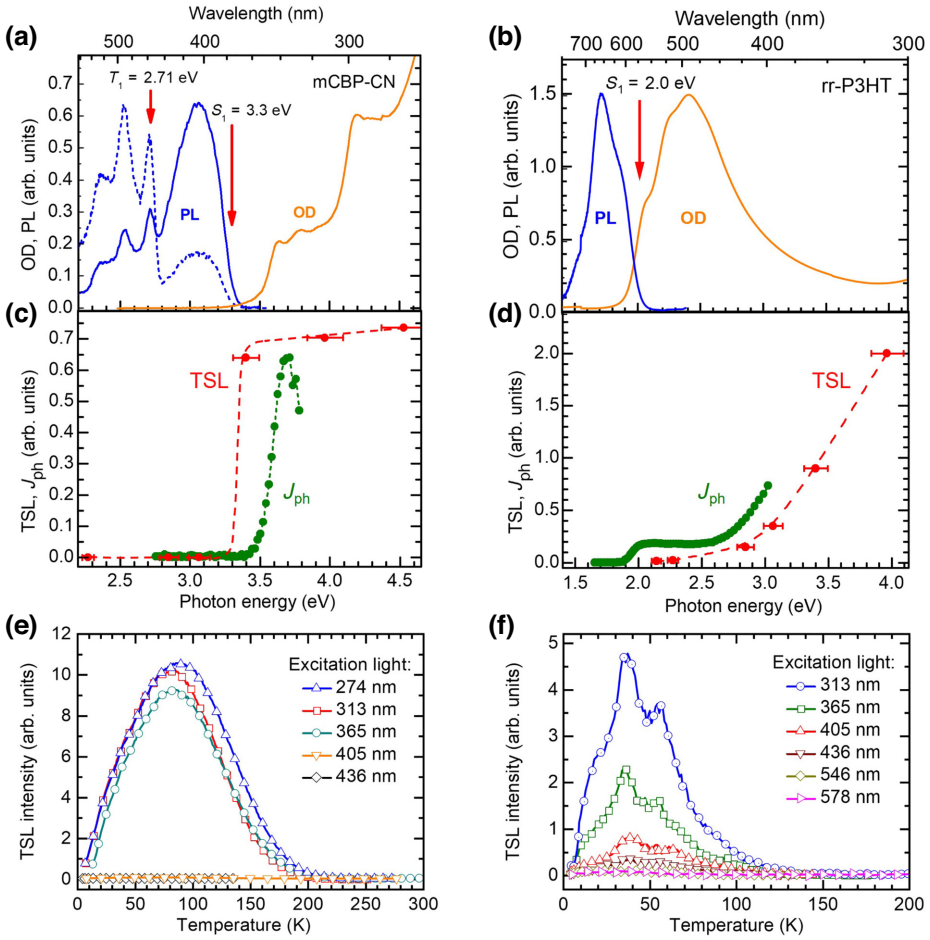

FIG. 2. (a) Absorption (orange solid line) where OD denotes optical density, low-temperature steady-state PL (blue solid line), and delayed emission (blue dashed line) of a mCBP-CN film measured at 77 K with a standard spectrofluorometer using a Xe lamp for excitation. The delayed emission is measured with 50-ms delay time after excitation and an integration time of 100 ms. (b) Absorption (orange solid line) and steady-state PL (blue solid line) measured at 77 K of a rr-P3HT film. (c) Dependence of the integrated TSL intensity upon the photon energy of excitation (red symbols) and PC action spectra (green symbols) of a mCBP-CN film; (d) action spectrum of TSL (red symbols) measured in this work as well as PC (green circles) adopted from Ref. [32] for rr-P3HT film. Dashed lines are a guide to the eye. (e) TSL glow curves of mCBP-CN film and of (f) a rr-P3HT film, both measured after excitation at 5 K with different photon energies of the cw-excitation light (wavelengths of the excitation are indicated in the figure).

As expected, in contrast to the mCBP-CN films, no phosphorescence component is found either in steady-state or delayed emission in rr-P3HT films even at low temperatures, owing to the negligible triplet state population in this system [28]. Figure 2(b) shows absorption spectra and cw-PL for a rr-P3HT film (orange and blue curves, respectively), exhibiting only fluorescence emission.

TSL in disordered organic semiconductors is known to originate from radiative recombination of spatially well separated trapped charge-carrier pairs created during photoexcitation of the sample at a low temperature [24,27]. The measured TSL curve itself is known to map a distribution of charge carriers localized within the lower-energy part of the intrinsic density of states (DOS). This technique allows determination of the width of the DOS σ_{DOS}, which has been found to be 151 meV in mCBP-CN films [27]. Action spectra of TSL (red circles) for mCBP-CN and rr-P3HT films are presented in Figs. 2(c) and 2(d), respectively. The TSL action spectra are obtained by plotting the integrated TSL intensity, calculated as the area under the TSL curves shown in Figs. 2(e) and 2(f), versus the photon excitation energy ($E_{h\upsilon}$). These action spectra demonstrate the fundamental difference in the TSL behavior between mCBP-CN and rr-P3HT. That is, there is a *significant energy offset* between the absorption edge and the action spectrum of TSL for rr-P3HT [Fig. 2(d)], while, in contrast, TSL intensity in mCBP-CN is virtually independent of $E_{h\upsilon}$ above the optical gap [Fig. 2(c)]. For rr-P3HT, the onset of the TSL action spectrum [Fig. 2(d)] is approximately 0.6–0.7 eV higher than the lowest singlet exciton state $S_1 = 2.0$ eV, which is in agreement with the exciton binding energy of 0.7 eV determined by Deibel *et al.* [32] from the combined spectrally resolved PC and photoemission measurements. This perfectly agrees with transient absorption measurements [28], showing that in single-layer P3HT devices the charge carriers are generated only from hot excitons and not from relaxed singlet exciton states. It is therefore reasonable to expect a similar offset for the TSL action spectrum. In contrast, the TSL intensity of the mCBP-CN films rises steeply at the optical gap and then appears to be remarkably *independent* of the energy of the excitation photons $E_{h\upsilon}$ above the optical gap [Figs. 2(c) and 2(e)]. mCBP-CN shows the same TSL signal even at zero excess photon energy of the exciting illumination with 365-nm light, i.e., within the lowest singlet S_1 state.

Figures 2(c) and 2(d) also present the action spectra of the PC (green circles) using photodiodes based on mCBP-CN (measured at 5 K) and rr-P3HT (measured at ambient temperature), respectively. The curves turn out to be similar to the action spectra of TSL. That is, for mCBP-CN, the PC rises sharply at the onset of absorption (some apparent decrease above 3.7 eV is due to absorption of the glass substrate covered with ITO and PEDOT:PSS layers). The PC is measured at a reverse bias of -7 V, which prevents electrode-sensitized photogeneration of charge carriers [35]. This indicates that the PC in mCBP-CN films is dominated by intrinsic bulk photogeneration, similar to the situation in TSL. In the photodiode made with rr-P3HT, we see a small PC component at the onset of absorption attributed to *extrinsic* dissociation, and the main onset at higher energies congruent with the electrical gap. The latter is the *intrinsic* PC resulting from autoionization that also produces the geminate pairs probed by the TSL signal.

The DF component seen in Fig. 2(a) (dashed blue curve) is spectrally identical to the prompt fluorescence (solid blue curve). This suggests the presence of a mechanism that involves triplet excitons, as demonstrated in the following. To elucidate the role of TTA in photophysical processes in the mCBP-CN films, we employ time-resolved PL measurements with pulsed nanosecond-laser excitation. Figure 3(a) shows the dependence of DF and phosphorescence intensity on variable laser excitation intensity for the mCBP-CN film at 5 K. The emission is recorded with a time delay of 2 ms after the laser excitation pulse at 355 nm (3.5 eV) and the gate width of 2 ms. The plotted emission intensities are obtained by integrating over the wavelength. The actual delayed emission spectra are presented in Fig. S1(a) of the Supplemental Material [36]. The phosphorescence intensity shows almost a square-root increase with increasing excitation laser power ($I_{\mathrm{ph}} \sim I_{\mathrm{exc}}^{m}$, where $m = 0.63$), implying that TTA is a dominant mechanism for depletion of the triplet reservoir in the range of laser intensities used in this experiment [37,38]. The DF intensity increases more steeply with increasing laser intensity, revealing an almost doubled exponent [37] with respect to the phosphorescence intensity increase ($m = 1.14$). The latter strongly suggests that DF emission is predominantly caused by TTA processes in this material.

Figure 3(b) presents the temperature dependence of the spectrally integrated phosphorescence intensity, DF intensity, and the PC (green triangles, blue squares, and red circles, respectively) measured from the same mCBP-CN film. As evident from Fig. 3(b), the phosphorescence intensity decreases monotonically with increasing temperature from 5 to 290 K. See Fig. S1(b) of the Supplemental Material [36] for the actual delayed emission spectra. In contrast, the DF detected in the same time slot of the ICCD detector first increases to its maximum intensity at around 110 K and then drops to an almost negligible level at room temperature. Note that the DF reaches its maximum intensity at a temperature T_{max} where the phosphorescence intensity is reduced to 50% of its value at 5 K. It should be emphasized that this type of temperature dependence peaking at an intermediate temperature is *very characteristic of DF* and was previously observed for DF in films of polyfluorene oligomers [39]. It has already been shown using a kinetic equation approach and kinetic Monte Carlo simulations [40] that the observed nonmonotonic temperature dependence of DF is a consequence

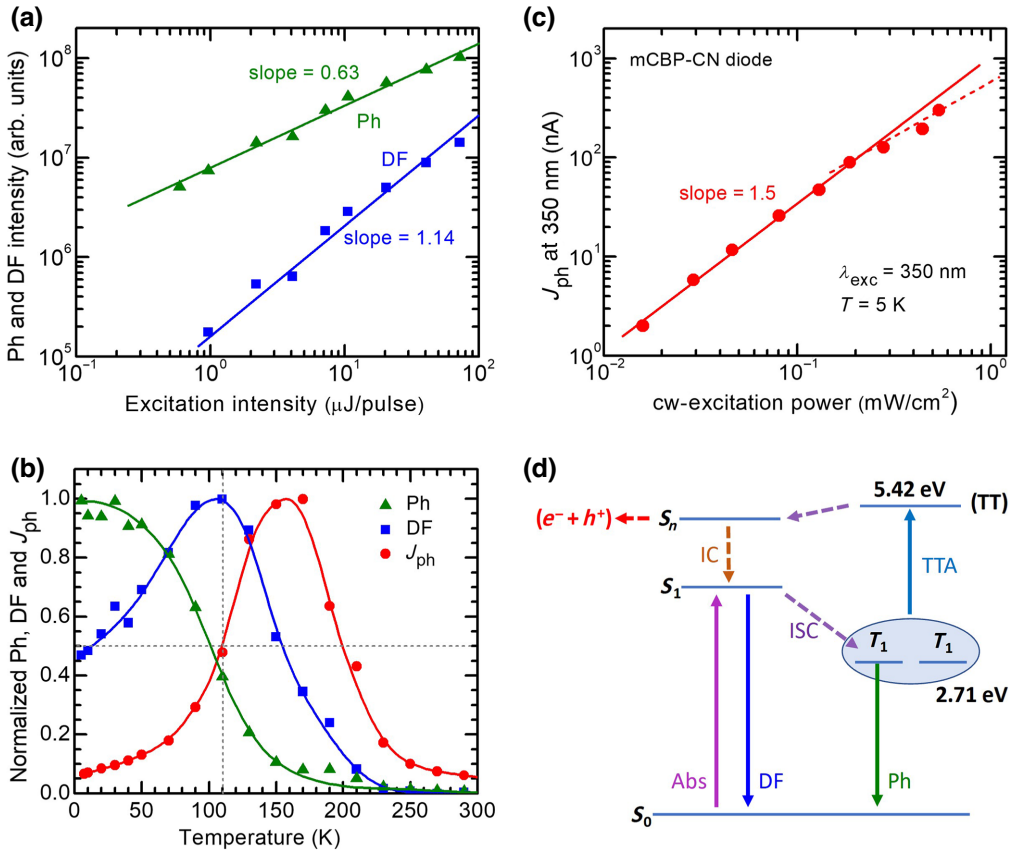

FIG. 3. Evidence for efficient TTA in mCBP-CN films: (a) dependence of spectrally integrated phosphorescence (Ph) (green triangles) and DF (blue squares) intensity on pulsed nanosecond-laser excitation intensity at 5 K, along with power-law fits to the data (solid line); (b) intensity of spectrally integrated Ph, DF, and PC (J_{ph}) versus temperature (symbols), along with guides to the eye (solid lines); (c) double-logarithmic plot of the PC vs cw-excitation intensity at 350 nm measured at 5 K (red circles). The observed supralinear dependence with slope 1.5 indicated by the red line is principally similar for the diode measured at both short-circuit and reverse bias (−7 V) conditions. (d) Suggested simplified energy diagram for the charge photogeneration process in mCBP-CN films, where IC and ISC denotes internal conversion and intersystem crossing, respectively.

of the temperature-dependent interplay between TTA and monomolecular quenching of the triplet excitations by quenching centers, controlled by thermally activated triplet exciton diffusion. At lower temperature, triplet diffusion causes TTA so that the phosphorescence is reduced and DF can be observed. The yield of this process increases with increasing temperature until the growing diffusion to quenching sites becomes sufficiently significant to reduce the triplet population and hence to curb the TTA process so that the DF falls off.

A similar nonmonotonic temperature dependence is also observed for the photocurrent J_{ph} measured in a mCBP-CN diode at very weak cw-excitation, which correlates with the temperature-dependent DF, although somewhat shifted towards higher temperatures [red circles, Fig. 3(b)]. The $J_{ph}(T)$ features a clear maximum at a moderately low temperature of around 170 K, followed by a drastic decrease in the PC up to room temperature. This suggests that the temperature dependence of the photocurrent $J_{ph}(T)$ is mostly governed by the TTA-UC-induced generation of the higher lying singlet state from which the geminate pairs are then generated, and less by a thermally activated field-assisted dissociation of these TTA-induced geminate pairs into free carriers. Figure 3(c) shows that the PC exhibits the supralinear dependence on cw-excitation power ($J_{ph} \propto I_{exc}^m$, where $m = 1.5$) measured in the range $0.016 < I_{exc} < 0.54$ mW/cm^2, i.e., under very low light fluences, evidencing that carrier photogeneration is a bimolecular process in this system. It is worth mentioning that a similar supralinear dependence with an exponent $m = 1.7$ was recently reported for a TTA-based up-converted fluorescence observed in virtually the same excitation power range $I_{exc} < 0.4$ mW/cm^2 in poly(styrene) nanoparticles doped with PtOEP and 9,10-diphenylanthracene [41]. Moreover, exponents of 1.47 to 1.57 have been reported for

TTA-induced enhanced PLDMR in nonfullerene acceptors (NFAs) and for TTA up-converted PL in bilayer NFA/rubrene systems, respectively [10,42]. The exact origin of such TTA behavior requires further investigation; however, Izawa and Hiramoto [42] have speculated that the value $m < 2$ may be attributed to some other parallel triplet quenching processes, such as triplet quenching by charge carriers.

The observed bimolecular character of the PC in mCBP-CN films [Fig. 3(c)], as well as the remarkable correlation between temperature dependences of the DF and the $J_{ph}(T)$ [Fig. 3b)], with both reaching a maximum value at moderately low temperatures and rolling off towards room temperatures, implies that the PC is governed by the TTA-UC-induced photogeneration of charge carriers. This mechanism is schematically depicted in Fig. 3(d): owing to the high energy of the lowest triplet state in mCBP-CN, the efficient TTA process can promote the energy UC to 5.42 eV (2.71 eV + 2.71 eV) and thus provides enough excitation energy to overcome the exciton binding energy, enabling autoionization to yield a separated electron (e^-) and hole (h^+) charge-carrier pair.

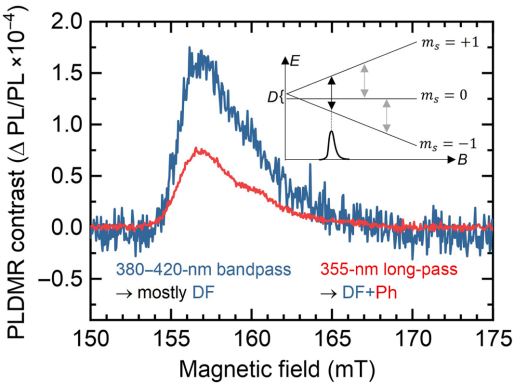

FIG. 4. PLDMR triplet spectra of fluorescence (380–420-nm bandpass filter, blue) and fluorescence plus phosphorescence (overall PL spectrum ≥355 nm, red). The bandpass-filtered DF-based spectrum shows increased PLDMR contrast (ΔPL/PL) in comparison to the long-pass-filtered spectrum that also probes phosphorescence. This is evidence that the PLDMR mostly stems from TTA-UC-induced DF rather than phosphorescence. The inset shows the probed $\Delta m_s = \pm 2$ triplet transition as a black arrow, in contrast to the gray arrows for the $\Delta m_s = \pm 1$ transitions.

B. PLDMR and LESR transient measurements

The TTA process in mCBP-CN films can be studied elegantly using PLDMR, as shown in Fig. 4. The principle of PLDMR investigations of triplet excitons and TTA is illustrated in Fig. S8 of the Supplemental Material [36]. Since TTA and the corresponding DF are spin-dependent, resonant microwave irradiation can modulate TTA probabilities and concomitantly the PL intensity. Figure 4 shows a positive (PL enhancing) half-field PLDMR spectrum at 10 K. In order to clarify how this triplet PLDMR signal is related to fluorescence and phosphorescence pathways, we measure it through either a 355-nm long-pass optical filter (transmitting both fluorescence and phosphorescence, red) or with a 380–420-nm bandpass filter (only the fluorescence component is transmitted, blue). Whilst keeping the measurement conditions the same, the bandpass-filtered spectrum (blue) shows a larger PLDMR contrast (ΔPL/PL). The total PL is reduced considerably when the phosphorescence component is blocked with the bandpass filter, while ΔPL changes less, leading to the increased contrast. However, the decisive factor is not the change in contrast, but that PLDMR is detected at all for the fluorescence component. Direct singlet fluorescence is spin-*independent*, while we observe spin-*dependent* fluorescence. This suggests the enhancement of the fluorescence component is related to a spin-dependent process, such as TTA-induced DF. The higher noise level of the bandpass curve (blue) in contrast to the long-pass curve (red) stems from dividing by the reduced PL intensity. Overall, these results testify that the TTA-induced DF process does take place in this material even at 10 K.

To gain a deeper insight into the *formation and recombination dynamics* of the trapped photogenerated charge carriers as well as the *lifetime of triplet excitons* in mCBP-CN films at low temperatures, we apply transient LESR. Since both triplets and charge carriers are paramagnetic excitations, they can be probed by LESR transient measurements, which complement the TSL measurements very well. In contrast to TSL, the ESR technique can potentially be used to estimate the concentration of *trapped charges*, as it results from direct microwave absorption by the paramagnetic species. Another distinguishing feature of LESR and PLDMR techniques is that, unlike TSL, they detect all charge carriers in the film regardless of whether they are generated via intrinsic or extrinsic mechanisms.

Figure 5(a) shows an example of the LESR spectrum of a neat mCBP-CN film at $g = 2$ ($\Delta m_s = \pm 1$, $S = 1/2$, see inset), which is due to photoinduced charge carriers recorded under steady-state 365-nm illumination at 10 K. No "dark" LESR signal is observed prior to illumination, excluding any impurity paramagnetic species. The multiple shoulders and secondary maxima in the low magnetic field region of the observed LESR signal are probably caused by hyperfine interactions of charge carriers with paramagnetic ^{14}N nuclei in mCBP-CN. The shape of this LESR spectrum is also found to depend on microwave power, as demonstrated in Fig. S3 of the Supplemental Material [36]. Another LESR component at $g = 4$ ($\Delta m_s = \pm 2$) is observed in the mCBP-CN film at half-field resonance, as shown in Fig. 5(b), which can only

arise for a total spin of $S > 1$. The position of the half-field signal suggests a high zero-field splitting, i.e., dipolar interaction, supporting the theory of molecular excitons with nearby spins as triplet excitons [43]. The observed LESR triplet spectrum in Fig. 5(b) corresponds to the same transition as the PLDMR spectrum shown in Fig. 4. Since a high zero-field splitting makes the signal in the full field ($\Delta m_s = \pm 1$) very broad, the signal intensity is too low to detect the spectrum in the full field (Fig. S9 of the Supplemental Material [36]). Note, the LESR spectra appear as first derivatives of the microwave absorption signals due to the used magnetic field modulation in contrast to PLDMR. A direct comparison of ESR and PLDMR spectra for charges ($S = 1/2$) and triplets ($S = 1$) is shown in Fig. S10 of the Supplemental Material [36].

This study focuses on the fact that, similar to the TSL, charge-related LESR signals in mCBP-CN films can be observed (i) upon photoexcitation within the S_1 state of this material, and (ii) only when photoexcitation occurs at low temperatures (see Fig. S7 of the Supplemental Material [36]). Moreover, no light-induced ESR signals are observed in neat rr-P3HT films, in agreement with our previous studies [44], indicating negligible charge-carrier photogeneration in rr-P3HT upon excitation within the absorption edge. These observations are perfectly correlated with the TSL excitation behavior for mCBP-CN and rr-P3HT films shown in Fig. 2, implying that the *same trapped charge carriers are responsible for both TSL and LESR phenomena*.

Figure 5(c) shows the temporal evolution of the LESR signal in mCBP-CN film at 10 K, which demonstrates the extremely slow LESR kinetics of both charge accumulation and charge recombination after ceasing the cw illumination. Interestingly, the LESR intensity gradually increases with exposure time, revealing no saturation even after a prolonged 60-min illumination (see Figs. S4–S6 and Note S1 of the Supplemental Material [36]). When the illumination is turned off, the LESR signal at 10 K decreases due to the recombination of charges following the $I_{\mathrm{LESR}} \sim -\log(t)$ decay kinetics measured over hours as shown in Fig. 5(e). This kinetic is indicative of dispersive charge recombination due to energy and/or spatial distribution of charge-carrier pairs and perfectly agrees with the isothermal recombination luminescence (IRL) (or long afterglow) decay kinetics $I_{\mathrm{IRL}} \sim -t^{-1}$ as depicted in Fig. S2 in the Supplemental Material [36] measured in the long delayed time limit after photoexcitation. This is because the LESR signal is proportional to the carrier concentration $I_{\mathrm{LESR}} \sim n$, whereas the IRL intensity is the first derivative of carrier concentration $I_{\mathrm{IRL}} \sim -dn/dt$ [45]. At elevated temperatures, the charge accumulation and recombination are accelerated, as expected, as demonstrated by the LESR transients for charges measured at temperatures 10, 50, and 100 K (Fig. S5 of the Supplemental Material [36]). The LESR results thus indicate that (i) the majority of photogenerated charges in mCBP-CN films under steady-state excitation at 10 K are metastable, originating from long-lived long-range geminate pairs, and (ii) no really fast charge recombination can be seen in these experiments because of the limited time resolution (100 ms) of the present LESR kinetics measurements.

In contrast to the very slow temporal evolution of the LESR signal caused by the recombination of charge carriers in Fig. 5(e), the LESR caused by triplets, as shown in Fig. 5(d), demonstrates fast increase, decrease, and saturation within seconds of switching the illumination on or off. The signal decrease as shown in Fig. 5(f) features exponential decay kinetics with a time constant $\tau = 1.7$ s. This value is comparable to the decay constant of the initial part of the isothermal afterglow measured at a constant temperature $T = 5$ K prior to the TSL heating run (Fig. S2 of the Supplemental Material [36]) and we ascribe it to the lifetime of triplet excitons in mCBP-CN films.

Thus, the PLDMR and LESR experiments demonstrate the abundance of charge carriers and triplet excitons being generated in mCBP-CN films upon photoexcitation within the absorption edge. In this regard, both methods show a high degree of similarity, as shown in Fig. S10 of the Supplemental Material [36].

C. Modeling of geminate-pair dissociation

It is obvious from the striking similarity between the temperature dependences of the DF and the PC [see Fig. 3(b)] that the PC is essentially determined (limited) by the same TTA process that determines the DF. Based on the experimental data presented in Sec. III A and the LESR data of Sec. III B, we suggest that TTA leads to the formation of a higher lying singlet state, $T_1 + T_1 \rightarrow S_n$. Autoionization from this state followed by thermalization leads to the formation of geminate pairs, $S_n \rightarrow (e^- \ldots h^+)$. These geminate pairs may have shorter or longer separation distances r_0 between the respective electron and hole. They will eventually dissociate by thermally activated and field-assisted diffusive hopping into free charges $(e^- \ldots h^+) \rightarrow (e^- + h^+)$. However, it still needs to be clarified to what extent the measured $J_{\mathrm{ph}}(T)$ is governed by the TTA-induced geminate-pair generation and to what extent it is governed by the dissociation of these geminate pairs into free carriers. Note that the PC is observed at low temperatures, and the geminate pairs are bound together by their Coulomb energy, which acts as an energy barrier for dissociation. This leads to a more general fundamental question: How does a photogenerated geminate pair dissociate into free carriers at such low temperatures, including liquid-helium temperature?

PC generation is a two-stage process and can therefore be expressed as a product of geminate-pair generation yield, which is a temperature-dependent quantity in the

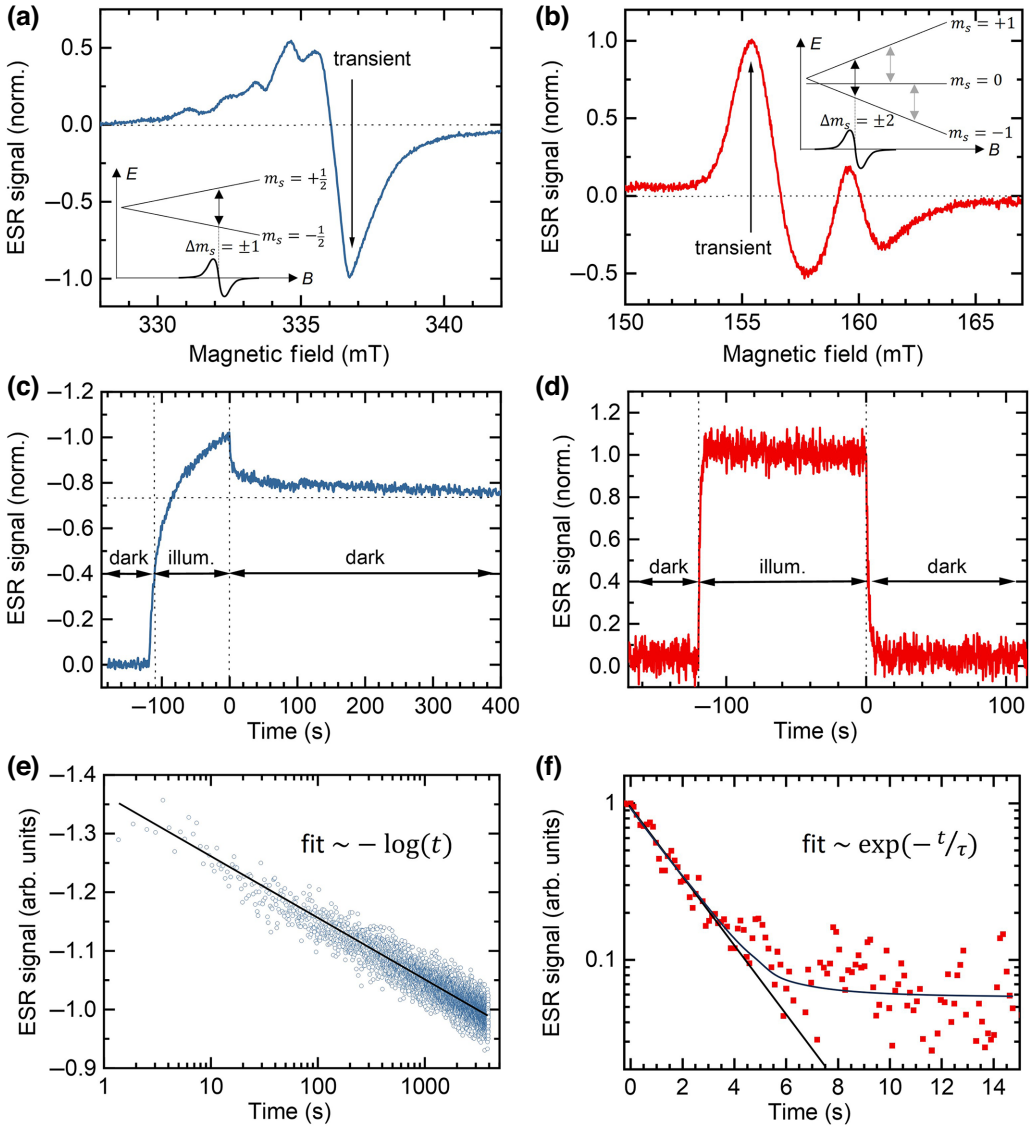

FIG. 5. Light-induced ESR of mCBP-CN under 365-nm excitation at 10 K due to charge carriers [blue lines or symbols in (a),(c),(e)] or triplets [red lines or symbols in (b),(d),(f)]. (a),(b) LESR signal as function of the applied magnetic field. The vertical arrows indicate the signal peaks where transients are measured. The insets show the Zeeman splitting of charge carriers or triplets and the probed $\Delta m_s = \pm 1$ and ± 2 ESR transitions, respectively. (c),(d) Illumination-dependent transient signal evolution. The signals grow upon illumination and decay in the dark with drastically different temporal behaviors. (e),(f) Semilog plots of the signal decays in the dark after terminating the excitation. For charges, a logarithmic time dependence $I_{\mathrm{LESR}} \sim -\log(t)$ is observed. Charges accumulate and decay over hours. For the triplet signal, an exponential decay $I_{\mathrm{LESR}} \sim \exp(-(t/\tau))$ with a time constant $\tau = 1.7$ s is observed.

case of TTA-facilitated autoionization $\Phi(T)$, and the probability of charge-pair dissociation $\eta(T)$ into free carriers. Hence, the entire process can be written as

$$T_1 + T_1 \rightarrow S_n \overset{\Phi(T)}{\rightarrow} (e^- \ldots h^+) \overset{\eta(T)}{\rightarrow} (e^- + h^+). \qquad (1)$$

Therefore, comparison of the DF and the PC measurements at various temperatures allows one to decouple the temperature-dependent geminate-pair generation $\Phi(T)$ and dissociation $\eta(T)$. Here we assume that $\Phi(T)$ is proportional to the measured temperature-dependent DF intensity, as both phenomena are induced by the same TTA process. The temperature dependence of the charge-pair dissociation probability can therefore be evaluated as $\eta(T) \propto J_{\mathrm{ph}}(T)/\Phi(T)$ [cf. Eq. (2) below] using the experimental data from Fig. 3(b) and is presented in Fig. 6(a) (black circles). As one can see, $\eta(T)$ demonstrates a clear nonexponential dependence when plotted in Arrhenius representation for the temperature ranging from 20 to 290 K. This implies that the classical disorder-free Onsager dissociation model is not applicable to amorphous organic semiconductors and should be extended to account for the

disorder that is known to assist the dissociation of photogenerated geminate pairs [46–50]. This is because the stronger the disorder is, the more easily the charge carriers can escape from the Coulomb potential since they are able to hop via localized states below the center of the DOS distribution, thereby requiring significantly less thermal energy. The shortcomings of the classical Onsager dissociation model have recently been solved in an extended model by Rubel *et al*. [46] that also accounts for the hopping motion involved in the dissociation process in a disordered system. Therefore, the dissociation probability $\eta(r_0, \tau, \sigma, T, E)$ is a function of the initial charge separation distance of the geminate pairs r_0, the lifetime of a geminate pair τ, the amount of energetic disorder in the material σ, temperature T, and electric field E. The PC then reads as follows:

$$J_{\mathrm{ph}}(T) \propto \Phi(T)\eta(r_0, \tau,\ \sigma, T, E). \tag{2}$$

To understand the observed temperature dependence of the dissociation yield $\eta(T)$, we use the analytical hopping model of Rubel *et al*. [46], which reproduces the Onsager and Frenkel field dependences of the dissociation probability as asymptotic cases. The model is based on a rate equation approach in a one-dimensional lattice of hopping sites where one charge is fixed (e.g., the electron) and the countercharge (e.g., the hole) executes a biased random walk in the presence of an external electric field and the Coulomb potential of the fixed charge. The mobile carrier will either recombine with the fixed charge at the origin, with a lifetime τ, or separate over a given distance $L = na$ to become free, where n is the number of lattice sites and a is the lattice constant. The temperature-dependent dissociation probability is

$$\eta(T) = 1 - \frac{\sum_{j=i}^{n-1} \nu_{j,j+1}^{-1} e^{(\varepsilon_j - \varepsilon_1/k_B T)}}{\tau + \sum_{j=1}^{n-1} \nu_{j,j+1}^{-1} e^{(\varepsilon_j - \varepsilon_1/k_B T)}}, \tag{3}$$

where i is the starting site of the mobile carrier ($i = 1$ corresponds to electron and hole being nearest neighbors with distance a), ε_j the site energies, k_B the Boltzmann constant, and $\nu_{j,j+1}$ the Miller-Abrahams hopping rates between nearest-neighbor sites j and $j + 1$, given by

$$\nu_{j,j+1} = \nu_0 e^{-2\gamma a} e^{-((\varepsilon_{j+1} - \varepsilon_j + |\varepsilon_{j+1} - \varepsilon_j|)/2k_B T)}, \tag{4}$$

with ν_0 the attempt-to-hop frequency and γ the inverse localization length. The on-site energies of the jth localized state at position $x_j = aj$,

$$\varepsilon_j = -\frac{q^2}{4\pi\epsilon_r\epsilon_0 x_j} - qEx_j + \varepsilon_j^0, \tag{5}$$

include the Coulomb binding energy, the potential energy drop due to the applied electric field E, and random Gaussian disorder ε_j^0 with standard deviation σ and mean value zero. q is the charge of the hole and ϵ_r, ϵ_0 the relative and vacuum permittivity, respectively. We have used $\epsilon_r = 3.5$, $\sigma = 0.1$ eV, $a = 1$ nm, $n = 100, E = 10^5$ V/cm, $\gamma = 2$ nm^{-1}, $\nu_0 = 10$ ps^{-1}, and computed the dissociation probability by averaging over 10^7 disorder realizations for different electron-hole initial separation distances $r_0 = ia$, where i is the integer number 1, 2, 3, 4, or 5. Note that although the latter option was included in the equation in the original Rubel model, it was not applied to compute the probability for different distances. Thus, the major advance we make using the model described here is that we also account for longer-distance geminate pairs.

In Fig. 6(a), we plot the dissociation probability of geminate electron-hole pairs ($e^- \ldots h^+$) normalized to the dissociation probability at 290 K. We use a lifetime for the pair of $\tau = 3 \times 10^4 t_0$, where $t_0 = e^{2\gamma a}/\nu_0$ is the minimum hopping time between isoenergetic sites. This lifetime corresponds to a value of around 164 ns for a minimum hopping time of about 5.5 ps. Importantly, we find that in order to reproduce the non-Arrhenius temperature dependence of the experimental data with a relatively steep activation energy at high temperatures (about 80 meV for $T \geq 150$ K) and nearly zero activation energy at low temperatures we need to include both short-distance pairs with $r_0 = 1$ nm and longer-distance pairs with $r_0 \geq 2$ nm. The short-distance pairs contribute to the high-temperature steep drop of the dissociation yield with decreasing T, while the longer-distance pairs account for the T-independent low-temperature part. Note that in the absence of electric field and energetic disorder, the thermal activation energy for the dissociation of nearest-neighbor pairs would be around 411 meV [Fig. 6(b)]. In the fit to the data presented in Fig. 6(a), approximately 97.0% of the charges are generated at $r_0 = 1$ nm, 2.9% at $r_0 = 2$ nm, and 0.1% at $r_0 = 3$ nm. The individual dissociation yields for $r_0 = 1, 2, 3, 4$, and 5 nm are shown in the Supplemental Material (Fig. S11) [36]. Satisfactory fits of the experimental data could also be obtained by considering different r_0 ratios, for example, 99.87% of the charges at $r_0 = 1$ nm and 0.13% at $r_0 = 5$ nm, or by considering a longer lifetime $\tau = 3 \times 10^6 t_0$ with 99% of the charges at $r_0 = 1$ nm and 1% at $r_0 = 5$ nm. However, they key common feature is that the vast majority of the geminate electron-hole pairs ($e^- \ldots h^+$) following autoionization from S_n are nearest neighbors and the minority are separated by intermediate distances. Figure 6(b) highlights the dramatic influence of disorder in assisting charge separation of short-distance Coulombically bound electron-hole pairs at low temperatures.

Finally, we emphasize that even though the long-distance geminate pairs seem to be only a small fraction of the total number of TTA-generated geminate pairs,

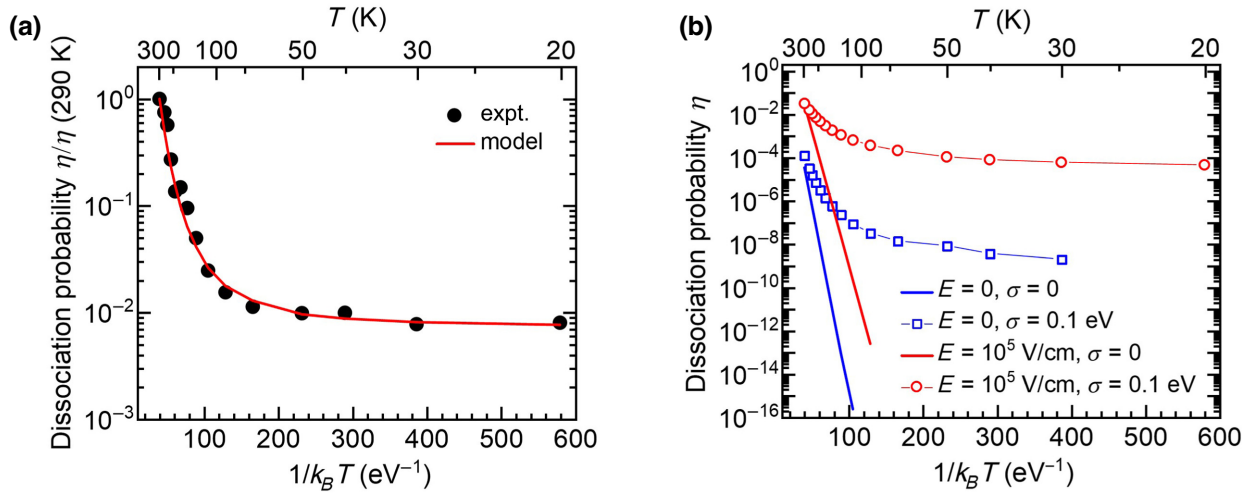

FIG. 6. (a) Arrhenius plot of the Onsager probability of charge dissociation extracted from the experimental data of Fig. 3(b) (black circles) and from the analytical hopping model (red curve) with the yield dissociation values normalized to the yield at 290 K. (b) Arrhenius plot of the dissociation probability of a short-distance electron-hole pair ($r_0 = 1$ nm) for a disordered (circles, squares) and a disorder-free (lines) system in the absence of electric field (blue line and squares) and in the presence of an electric field (red line and circles).

their abundance in mCBP-CN films is unambiguously testified by the strong isothermal afterglow (Fig. S2 in the Supplemental Material [36]), the TSL, and the LESR signals observed under photoexcitation at 10 K. The presented LESR kinetics cannot probe the nearest-neighbor charge pairs as their lifetime is shorter than the time resolution of the LESR kinetic measurements (limited by the 100-ms lock-in time constant). Note that any intermediate short-lived pairs can be probed on (sub-)microsecond timescales only with transient LESR upon pulsed nanosecond-laser excitation, as has been demonstrated for bulk heterojunction photovoltaic systems [51,52]. Furthermore, the ESR signal shape for those close pairs is expected to be broader due to enhanced short-range dipolar interaction in comparison to the spectra presented in Fig. 5(a).

IV. DISCUSSION

We briefly discuss the reason for the occurrence of a pronounced maximum in the DF intensity at a certain temperature [cf. Fig. 3(c), blue curve]. A similar effect has been studied in detail for a series of poly(*p*-phenylene) oligomers [39] and it was found to be a consequence of thermally activated triplet exciton diffusion toward quenching sites in a disordered organic solid. Even in well purified compounds, there may be some residual amount of structural or chemical defects capable of quenching triplet excitons due to their long lifetime. The triplet quenching in the mCBP-CN films is evidenced by the observed drastic decrease of phosphorescence with increasing temperature [Fig. 3(c), green curve], which drops to a negligible level at room temperature. Considering that both the bimolecular TTA and monomolecular triplet quenching are diffusion-controlled processes, their interplay leads to the situation that the number of TTA events peaks at a certain temperature [40]. Indeed, triplet quenching is negligible at zero temperature and the DF tends to increase with temperature due to the temperature-dependent diffusivity [53] promoting the collision of two triplets until the triplet quenching rate (which also increases with temperature) equals the intrinsic decay rate [39,40]. From that point on, further increases of temperature lead to a progressive decrease in TTA probability, since the triplet population is reduced by quenching, and concomitantly, the DF intensity falls. In between, the DF features a maximum, and the peak temperature is determined by various material parameters—in particular, by the quencher concentration and the energy disorder. The disorder has been shown to reduce triplet diffusivity, resulting in a shift in the DF maximum towards higher temperatures [40].

A key finding of our study is that, similar to the DF intensity, the intrinsic PC in mCBP-CN diodes exhibits a similar prominent maximum at an intermediate temperature followed by a drastic decrease with temperature upon approaching room temperature [Fig. 3(c), red curve]. Such a decrease with temperature is an unusual behavior for a PC in a disordered system. It suggests that the temperature-dependent bimolecular TTA process governs the intrinsic charge-carrier generation and, consequently, the PC in these films. This is further proven by observation of the supralinear dependence of the PC on cw-excitation power [Fig. 3(c)] at very low excitation power (below 1 mW/cm^2).

The high-efficiency TTA process observed in mCBP-CN thin films is not self-evident for a single-component

heavy-atom-free system. We attribute this behavior to a combination of several factors. Firstly, the relatively high ISC rate estimated for mCBP-CN films, $k_{ISC} = 1.8 \times 10^8\ s^{-1}$, is expected in accordance with the El-Sayed rule, since it involves a change of orbital type from a singlet state with a charge-transfer character to a triplet state localized on the biphenyl moiety. Secondly, a relatively low concentration of quenching centers and the high energy of the lowest triplet state ($T_1 = 2.71$ eV) in mCBP-CN gives rise to a very long triplet lifetime, as found by LESR studies [Fig. 5(d)], which is around 2 s, because the nonradiative rate is greatly reduced in accordance with the energy gap law. These factors can provide a large triplet excitation density in this material under steady-state photoexcitation. In contrast to mCBP-CN, rr-P3HT is not a phosphorescent material due to slow ISC from the lowest singlet state to the T_1 state, as confirmed by transient absorption measurements [28], which revealed no measurable triplet formation in rr-P3HT films under excitation at the absorption band edge. Moreover, the low energy of the lowest triplet exciton state $T_1 = 1.55$ eV for rr-P3HT film [28] is expected to enhance the nonradiative decay rate of triplets in this material.

Further, spin-coated mCBP-CN films are typically amorphous and thus quite disordered. The energetic disorder for charge carriers was found to be about 150 meV [27] and it is dominated by the dipolar-disorder contribution. The energy landscape for triplets is naturally less disordered. In the present work, we estimate a triplet exciton DOS width of about $\sigma_{triplet} = 37$ meV based on the Gaussian width of the 0–0 peak in the phosphorescence spectra presented in Fig. 2(a). For details of the Gaussian fit to the 0–0 peak, see Fig. S12 of the Supplemental Material [36]. This width of the DOS likely results from the significant conformational disorder due to the conformational freedom and presence of soft dihedral angles in this organic material [54]. Recent kinetic Monte Carlo simulations by Saxena *et al*. [40] have demonstrated that the energetic disorder is crucial for obtaining a high yield of TTA because it causes filamentary triplet transport in disordered solids; thus, it locally enhances triplet densities and the probability of two triplets encountering each other rather than an impurity.

Another principal finding of this work is that the dissociation probability $\eta(T)$ of photoinduced charge pairs is almost *temperature-independent* at low temperatures in the range up to $T \leq 100$ K [Fig. 6(a)]. This cannot be rationalized by a classical "disorder-free" Onsager model predicting an exponential drop of the geminate-pair dissociation yield with decreasing temperature, as demonstrated in Fig. 6(b) (straight lines). At higher temperatures, $\eta(T)$ reveals some thermally activated behavior featuring an activation energy of around 80 meV. The latter is responsible for the notable shift of the maximum $J_{ph}(T)$ with respect to the temperature of maximal DF intensity (i.e., maximum of TTA efficiency) [Fig. 3(b)], which proves that the charge dissociation in the range of moderately high temperatures does require extra thermal energy. We demonstrate that the puzzle can be resolved within the charge dissociation model by Rubel *et al*. [46] by accounting for the presence of energetic disorder, which *dramatically facilitates the separation* of charges, particularly at low temperatures [Fig. 6(b)]. Although previous hopping transport theories and relevant computer simulations [46–48] have shown that the disorder greatly weakens the temperature dependence of the geminate-pair dissociation yield under the applied electric field, they have never been applied to describe PCs in such a low-temperature limit approaching liquid helium temperature. It is remarkable that the Rubel model [46] is found to describe the temperature-dependent PC so well across a broad temperature range from 300 down to 5 K [Fig. 6(a)] by considering a distribution of initial charge separation distances of the geminate pairs. This means that the presence of energetic disorder and energy barriers for back charge recombination, which result in substantially long lifetimes of photogenerated geminate charge pairs and slow recombination, must be taken into consideration. Experimental evidence of very slow charge recombination at 10 K is provided by extremely slow LESR and the afterglow decay kinetics presented in Fig. 5(c) and Fig. S2 (in the Supplemental Material [36]), respectively.

V. CONCLUSIONS

In this study, we demonstrate, that similar to the DF, the intrinsic photogeneration of geminate pairs of charge carriers in a single-component mCBP-CN film is dominated by the TTA-induced UC process. Energetically, this is easily feasible due to the high energy of the lowest triplet state in mCBP-CN. As a result, the TTA process can readily promote energy up-conversion to 5.42 eV [Fig. 3(d)], which provides plenty of excess energy to overcome the exciton binding energy, which is known to be within the range of 0.5–1 eV for small molecule semiconductors. The autoionization of the TTA-UC-generated high-energy neutral excited state is the major cause of the charge photogeneration observed in this material.

This photogeneration mechanism requires a high concentration of long-lived triplets that enable a highly efficient TTA process. This is not a trivial issue for a single-component material that does not contain a heavy atom. We attribute the efficient TTA process in mCBP-CN to efficient ISC, a high triplet energy level (2.71 eV), very long-lived triplet excitations (about 2 s) with a low quenching rate, and the presence of energy disorder that locally enhances the triplet densities. The photocurrent measured in an mCBP-CN diode shows an unusual temperature dependence $J_{ph}(T)$: (i) it is observed primarily at low temperatures peaking at around 170 K and rolls off

significantly at higher temperatures, and (ii) $J_{ph}(T)$ shows a striking correlation with the temperature dependence of the delayed fluorescence. We take this temperature dependence to suggest that triplet fusion is a common origin for both processes. This conclusion is affirmed by a supralinear dependence of the PC on excitation intensity observed even at very low excitation power (below 1 mW/cm^2), implying a bimolecular nature of the charge-generation process. Quantitative modeling of the PC using a hopping transport formalism indeed confirms that the temperature-dependent yield of free charges is mainly determined by the TTA process that forms the high-lying singlet state, and not by the dissociation probability from that high-lying singlet state. To obtain the correct temperature dependence, it is essential to account for the energy disorder and a distribution of initial charge separation distances.

We would like to highlight the importance of energy disorder, which actually plays a twofold beneficial role in the above TTA-UC-induced PC generation. The disorder of the triplet exciton states and that of the charge states in mCBP-CN films is found to be around 37 and 150 meV, respectively. First, the disorder of the excitonic state has previously been shown [40] to locally enhance triplet densities. This local enhancement should facilitate the TTA efficiency in mCBP-CN. It is worth noting that, to achieve a desirable shift of maximal TTA efficiency to room temperature, a somewhat larger triplet DOS width of at least 70 meV is required, as well as a triplet quencher density as small as about 10^{17} cm^{-3} [40]. This might be accomplished by proper selection of organic semiconductor materials and improved material purification and/or encapsulation to reduce the concentration of triplet quenchers, e.g., molecular oxygen. Second, in this work we demonstrate that the disorder of a charged state can have a dramatic influence in assisting the charge separation of Coulombically bound electron-hole pairs at low temperatures, [Fig. 6(b)]. Organic perfect single crystals may not exhibit this disorder-assisted dissociation mechanism. We find that the disorder-based dissociation model of Rubel *et al.* [46] describes remarkably well the dissociation yield over the entire broad temperature range 5–300 K [Fig. 6(a)] if one also accounts for the distribution of geminate-pair radii. Our TSL and LESR measurements clearly prove photogeneration of a significant amount of charge pairs with an intrapair separation of several intermolecular distances. Hence, TTA can lead to the formation of a high-lying singlet state and subsequent formation of long-range geminate pairs that separate into free carriers with virtually no activation energy and that provide an intrinsic photocurrent at the onset of absorption even at temperatures as low as 5 K. It also explains the counterintuitive finding that the level of stationary photocurrent in this disordered material at 5 K is almost the same as at room temperature. Finally, we wish to point out that the mechanism of geminate-pair photogeneration through the TTA-UC process discussed in this paper is not exclusive to mCBP-CN; it may be applicable to other organic semiconductors that possess an efficient ISC and a sufficiently high triplet energy level (e.g., carbazole- or triazine-based compounds), the TSL of which we studied previously [24,25].

ACKNOWLEDGMENTS

The authors acknowledge funding through the EU Marie Skłodowska-Curie Innovative Training Network (ITN) "TADFsolutions" grant (Project No. 101073045) and "TADFlife" (Grant No. 812872) as well as the Volkswagen Foundation. This research was also supported by the Deutsche Forschungsgemeinschaft (DFG, German Research Foundation) through the project "MARS" (Grant No. KO 3973/8-1), and by the Ministry of Education and Science of Ukraine through an external aid instrument for the fulfillment of Ukraine's commitments under the EU Framework Programme "Horizon 2020" (Project No. 18). J.G., A.S., and V.D. acknowledge support by the Deutsche Forschungsgemeinschaft (DFG, German Research Foundation) within the Research Training School "Molecular biradicals: Structure, properties and reactivity" (Grant No. GRK2112) and the Bavarian Network "Solar Technologies Go Hybrid".

[1] S. Baluschev, T. Miteva, V. Yakutkin, G. Nelles, A. Yasuda, and G. Wegner, Up-conversion fluorescence: Noncoherent excitation by sunlight, Phys. Rev. Lett. **97**, 143903 (2006).

[2] P. Bharmoria, H. Bildirir, and K. Moth-Poulsen, Triplet–triplet annihilation based near infrared to visible molecular photon upconversion, Chem. Soc. Rev. **49**, 6529 (2020).

[3] T. Schloemer, P. Narayanan, Q. Zhou, E. Belliveau, M. Seitz, and D. N. Congreve, Nanoengineering triplet–triplet annihilation upconversion: From materials to real-world applications, ACS Nano **17**, 3259 (2023).

[4] H. Goudarzi, L. Koutsokeras, A. H. Balawi, C. Sun, G. K. Manolis, N. Gasparini, Y. Peisen, G. Antoniou, S. Athanasopoulos, and C. C. Tselios, Microstructure-driven annihilation effects and dispersive excited state dynamics in solid-state films of a model sensitizer for photon energy up-conversion applications, Chem. Sci. **14**, 2009 (2023).

[5] R. Karpicz, S. Puzinas, V. Gulbinas, A. Vakhnin, A. Kadashchuk, and B. P. Rand, Exciton dynamics in an energy up-converting solid state system based on diphenylanthracene doped with platinum octaethylporphyrin, Chem. Phys. **429**, 57 (2014).

[6] P. C. Chow, S. Gélinas, A. Rao, and R. H. Friend, Quantitative bimolecular recombination in organic photovoltaics through triplet exciton formation, J. Am. Chem. Soc. **136**, 3424 (2014).

[7] C. Gärtner, C. Karnutsch, U. Lemmer, and C. Pflumm, The influence of annihilation processes on the threshold current

density of organic laser diodes, J. Appl. Phys. **101**, 023107 (2007).

[8] D. Stich, F. Späth, H. Kraus, A. Sperlich, V. Dyakonov, and T. Hertel, Triplet–triplet exciton dynamics in single-walled carbon nanotubes, Nat. Photonics **8**, 139 (2014).

[9] T. Dilbeck and K. Hanson, Molecular photon upconversion solar cells using multilayer assemblies: Progress and prospects, J. Phys. Chem. Lett. **9**, 5810 (2018).

[10] L. J. Hart, J. Grüne, W. Liu, T. k. Lau, J. Luke, Y. C. Chin, X. Jiang, H. Zhang, D. J. Sowood, and D. M. Unson, Understanding the role of triplet-triplet annihilation in nonfullerene acceptor organic solar cells, Adv. Energy Mater. **13**, 2301357 (2023).

[11] D. W. Gehrig, I. A. Howard, and F. Laquai, Charge carrier generation followed by triplet state formation, annihilation, and carrier recreation in PBDTTT-C/PC60BM photovoltaic blends, J. Phys. Chem. C. **119**, 13509 (2015).

[12] N. A. Kukhta, T. Matulaitis, D. Volyniuk, K. Ivaniuk, P. Turyk, P. Stakhira, J. V. Grazulevicius, and A. P. Monkman, Deep-blue high-efficiency TTA OLED using para-and meta-conjugated cyanotriphenylbenzene and carbazole derivatives as emitter and host, J. Phys. Chem. Lett. **8**, 6199 (2017).

[13] H. Lim, S. J. Woo, Y. H. Ha, Y. H. Kim, and J. J. Kim, Breaking the efficiency limit of deep-blue fluorescent OLEDs based on anthracene derivatives, Adv. Mater. **34**, 2100161 (2022).

[14] J. Grüne, N. Bunzmann, M. Meinecke, V. Dyakonov, and A. Sperlich, Kinetic modeling of transient electroluminescence reveals TTA as an efficiency-limiting process in exciplex-based TADF OLEDs, J. Phys. Chem. C. **124**, 25667 (2020).

[15] A. Monguzzi, A. Oertel, D. Braga, A. Riedinger, D. K. Kim, P. N. Knusel, A. Bianchi, M. Mauri, R. Simonutti, and D. J. Norris, Photocatalytic water-splitting enhancement by subbandgap photon harvesting, ACS Appl. Mater. Interfaces **9**, 40180 (2017).

[16] G. Antoniou, P. Yuan, L. Koutsokeras, S. Athanasopoulos, D. Fazzi, J. Panidi, D. G. Georgiadou, T. Prodromakis, and P. E. Keivanidis, Low-power supralinear photocurrent generation via excited state fusion in single-component nanostructured organic photodetectors, J. Mater. Chem. C **10**, 7575 (2022).

[17] A. Kadashchuk, Y. Skryshevskii, A. Vakhnin, N. Ostapenko, V. Arkhipov, E. Emelianova, and H. Bässler, Thermally stimulated photoluminescence in disordered organic materials, Phys. Rev. B **63**, 115205 (2001).

[18] C. Carati, L. Bonoldi, and R. Po, Density of trap states in organic photovoltaic materials from LESR studies of carrier recombination kinetics, Phys. Rev. B **84**, 245205 (2011).

[19] J. M. Cho, D. S. Kim, S. Bae, S.-J. Moon, W. S. Shin, D. H. Kim, S. H. Kim, A. Sperlich, S. Väth, and V. Dyakonov, Light-induced electron spin resonance study of galvinoxyl-doped P3HT/PCBM bulk heterojunctions, Org. Electron. **27**, 119 (2015).

[20] A. Kadashchuk, Y. Skryshevski, Y. Piryatinski, A. Vakhnin, E. Emelianova, V. Arkhipov, H. Bässler, and J. Shinar, Thermally stimulated photoluminescence in poly(2, 5-dioctoxy p-phenylene vinylene), J. Appl. Phys. **91**, 5016 (2002).

[21] S. Kuroda, K. Marumoto, Y. Shimoi, and S. Abe, ESR spectroscopy of polarons in conjugated electroluminescent polymers, Thin Solid Films **393**, 304 (2001).

[22] A. Köhler, D. Dos Santos, D. Beljonne, Z. Shuai, J.-L. Brédas, A. B. Holmes, A. Kraus, K. Müllen, and R. H. Friend, Charge separation in localized and delocalized electronic states in polymeric semiconductors, Nature **392**, 903 (1998).

[23] A. Kadashchuk, V. I. Arkhipov, C.-H. Kim, J. Shinar, D.-W. Lee, Y.-R. Hong, J.-I. Jin, P. Heremans, and H. Bässler, Localized trions in conjugated polymers, Phys. Rev. B **76**, 235205 (2007).

[24] A. Kadashchuk, A. Vakhnin, Y. Skryshevski, V. Arkhipov, E. Emelianova, and H. Bässler, Thermally stimulated luminescence in π-conjugated polymers containing fluorene and spirobifluorene units, Chem. Phys. **291**, 243 (2003).

[25] A. Stankevych, R. Saxena, A. Vakhnin, F. May, N. Kinaret, D. Andrienko, J. Genoe, H. Bässler, A. Köhler, and A. Kadashchuk, Monitoring the charge-carrier-occupied density of states in disordered organic semiconductors under nonequilibrium conditions using thermally stimulated luminescence spectroscopy, Phys. Rev. Appl. **19**, 054007 (2023).

[26] A. Kadashchuk, R. Schmechel, H. von Seggern, U. Scherf, and A. Vakhnin, Charge-carrier trapping in polyfluorene-type conjugated polymers, J. Appl. Phys. **98**, 024101 (2005).

[27] A. Stankevych, A. Vakhnin, D. Andrienko, L. Paterson, J. Genoe, I. Fishchuk, H. Bässler, A. Köhler, and A. Kadashchuk, Density of states of OLED host materials from thermally stimulated luminescence, Phys. Rev. Appl. **15**, 044050 (2021).

[28] J. Guo, H. Ohkita, H. Benten, and S. Ito, Near-IR femtosecond transient absorption spectroscopy of ultrafast polaron and triplet exciton formation in polythiophene films with different regioregularities, J. Am. Chem. Soc. **131**, 16869 (2009).

[29] G. F. Burkhard, E. T. Hoke, and M. D. McGehee, Accounting for interference, scattering, and electrode absorption to make accurate internal quantum efficiency measurements in organic and other thin solar cells, Adv. Mater. **22**, 3293 (2010).

[30] B. A. Naqvi, M. Schmid, E. Crovini, P. Sahay, T. Naujoks, F. Rodella, Z. Zhang, P. Strohriegl, S. Bräse, E. Zysman-Colman, and Wolfgang Brütting, What controls the orientation of TADF emitters?, Front. Chem. **8**, 750 (2020).

[31] S. Nešpůrek, F. Schauer, and A. Kadashchuk, Visible photoluminescence in polysilanes, Monatsh. Chem. **132**, 159 (2001).

[32] C. Deibel, D. Mack, J. Gorenflot, A. Schöll, S. Krause, F. Reinert, D. Rauh, and V. Dyakonov, Energetics of excited states in the conjugated polymer poly(3-hexylthiophene), Phys. Rev. B **81**, 085202 (2010).

[33] S. A. Bagnich, A. Rudnick, P. Schroegel, P. Strohriegl, and A. Köhler, Triplet energies and excimer formation in meta-

and para-linked carbazolebiphenyl matrix materials, Philos. Trans. R. Soc., A **373**, 20140446 (2015).

[34] S. A. Bagnich, S. Athanasopoulos, A. Rudnick, P. Schroegel, I. Bauer, N. C. Greenham, P. Strohriegl, and A. Köhler, Excimer formation by steric twisting in carbazole and triphenylamine-based host materials, J. Phys. Chem. C **119**, 2380 (2015).

[35] S. Barth and H. Bässler, Intrinsic photoconduction in PPV-type conjugated polymers, Phys. Rev. Lett. **79**, 4445 (1997).

[36] See the Supplemental Material at http://link.aps.org/supplemental/10.1103/PhysRevApplied.20.064029 for an explanation for the lack of saturation of the LESR signals with increasing exposure time (Note S1); more results of PL, TSL, LESR, and PLDMR measurements (Figs. S1–S10); calculated charge dissociation yield for different initial electron-hole separation distances (Fig. S11); and for an estimate of the triplet exciton DOS width (Fig. S12).

[37] D. Hertel, H. Bässler, R. Guentner, and U. Scherf, Triplet-triplet annihilation in a poly(fluorene)-derivative, J. Chem. Phys. **115**, 10007 (2001).

[38] V. Jankus, E. W. Snedden, D. W. Bright, V. L. Whittle, J. Williams, and A. Monkman, Energy upconversion via triplet fusion in super yellow PPV films doped with palladium tetraphenyltetrabenzoporphyrin: A comprehensive investigation of exciton dynamics, Adv. Funct. Mater. **23**, 384 (2013).

[39] S. T. Hoffmann, J.-M. Koenen, U. Scherf, I. Bauer, P. Strohriegl, H. Bässler, and A. Köhler, Triplet–triplet annihilation in a series of poly(*p*-phenylene) derivatives, J. Phys. Chem. B. **115**, 8417 (2011).

[40] R. Saxena, T. Meier, S. Athanasopoulos, H. Bässler, and A. Köhler, Kinetic Monte Carlo study of triplet-triplet annihilation in conjugated luminescent materials, Phys. Rev. Appl. **14**, 034050 (2020).

[41] S.-Y. Hwang, D. Song, E.-J. Seo, F. Hollmann, Y. You, and J.-B. Park, Triplet–triplet annihilation-based photon-upconversion to broaden the wavelength spectrum for photobiocatalysis, Sci. Rep. **12**, 9397 (2022).

[42] S. Izawa and M. Hiramoto, Efficient solid-state photon upconversion enabled by triplet formation at an organic semiconductor interface, Nat. Photonics **15**, 895 (2021).

[43] S. S. Eaton, K. M. More, B. M. Sawant, and G. R. Eaton, Use of the ESR half-field transition to determine the interspin distance and the orientation of the interspin vector in systems with two unpaired electrons, J. Am. Chem. Soc. **105**, 6560 (1983).

[44] A. Sperlich, H. Kraus, C. Deibel, H. Blok, J. Schmidt, and V. Dyakonov, Reversible and irreversible interactions of poly(3-hexylthiophene) with oxygen studied by spin-sensitive methods, J. Phys. Chem. B **115**, 13513 (2011).

[45] R. Chen, Methods for kinetic analysis of thermally stimulated processes, J. Mater. Sci. **11**, 1521 (1976).

[46] O. Rubel, S. Baranovskii, W. Stolz, and F. Gebhard, Exact solution for hopping dissociation of geminate electron-hole pairs in a disordered chain, Phys. Rev. Lett. **100**, 196602 (2008).

[47] E. Emelianova, M. Van der Auweraer, and H. Bässler, Hopping approach towards exciton dissociation in conjugated polymers, J. Chem. Phys. **128**, 224709 (2008).

[48] U. Albrecht and H. Bässler, Yield of geminate pair dissociation in an energetically random hopping system, Chem. Phys. Lett. **235**, 389 (1995).

[49] S. Athanasopoulos, H. Bässler, and A. Köhler, Disorder vs delocalization: Which is more advantageous for high-efficiency organic solar cells?, J. Phys. Chem. Lett. **10**, 7107 (2019).

[50] S. Athanasopoulos, F. Schauer, V. Nádaždy, M. Weiß, F. J. Kahle, U. Scherf, H. Bässler, and A. Köhler, What is the binding energy of a charge transfer state in an organic solar cell?, Adv. Energy Mater. **9**, 1900814 (2019).

[51] J. Niklas, S. Beaupre, M. Leclerc, T. Xu, L. Yu, A. Sperlich, V. Dyakonov, and O. G. Poluektov, Photoinduced dynamics of charge separation: From photosynthesis to polymer–fullerene bulk heterojunctions, J. Phys. Chem. B. **119**, 7407 (2015).

[52] J. Behrends, A. Sperlich, A. Schnegg, T. Biskup, C. Teutloff, K. Lips, V. Dyakonov, and R. Bittl, Direct detection of photoinduced charge transfer complexes in polymer fullerene blends, Phys. Rev. B **85**, 125206 (2012).

[53] S. T. Hoffmann, S. Athanasopoulos, D. Beljonne, H. Bässler, and A. Köhler, How do triplets and charges move in disordered organic semiconductors? A Monte Carlo study comprising the equilibrium and nonequilibrium regime, J. Phys. Chem. C. **116**, 16371 (2012).

[54] A. Mondal, L. Paterson, J. Cho, K.-H. Lin, B. van der Zee, G.-J. A. Wetzelaer, A. Stankevych, A. Vakhnin, J.-J. Kim, and A. Kadashchuk, Molecular library of OLED host materials—Evaluating the multiscale simulation workflow, Chem. Phys. Rev. **2**, 031304 (2021).